Available online at www.sciencedirect.com
ScienceDirect
Comput. Methods Appl. Mech. Engrg. 396 (2022) 115044
Computer methods in applied mechanics and engineering
www.elsevier.com/locate/cma

A modular nonlinear stochastic finite element formulation for uncertainty estimation

Yanis Ammouche, Antoine Jérusalem*

Department of Engineering Science, University of Oxford, Parks Road, Oxford, OX1 3PJ, UK

Received 6 October 2021; received in revised form 20 April 2022; accepted 21 April 2022
Available online 25 May 2022

Abstract

The Monte Carlo method is widely used for the estimation of uncertainties in mechanical engineering design. However, while flexible, this method remains impractical in terms of computational time and scalability. To bypass these limitations, other more efficient approaches such as the Galerkin stochastic finite element method (GSFEM) or the collocation method have been proposed. GSFEM provides accurate output statistics, has the advantage of being sampling independent and can be modular in terms of operations, albeit code intrusive. While linear elasticity has been extensively covered in the literature, the application of GSFEM to nonlinear mechanical behaviour remains relatively unexplored, in part due to the difficulty to capture nonlinear effects with the traditional GSFEM interpolants. To this end, we propose a seamless and efficient modular framework avoiding the need to know a priori the material law. In particular, the method makes use of a wavelet based formulation able to capture simultaneously continuous and discontinuous behaviours, and stochastic operators are proposed to straightforwardly adapt any material model. Finally, the flexibility of this approach is illustrated with two problems: (i) a 3D hyperelastic example with nonlinear behaviour arising from buckling uncertainty, and (ii) the evaluation of the displacement of a point within a structure based on how much of the external accessible structural deformation is known.

Keywords: Uncertainty quantification; Stochastic finite element method; Wavelets

1. Introduction

Manufacturing processes, however controlled they might be, are inherently suffering from a given degree of mechanical properties and geometrical uncertainties. For example, high pressure die casting, one of the most utilised manufacturing processes for light metals such as aluminium and magnesium alloys, is known for its high productivity, high dimensional accuracy and excellent mechanical properties. However, due to turbulence and limited shrinkage feeding capability, defects such as entrapped air and shrinkage porosity formed in castings eventually affect the stability of mechanical properties [1]. The variability of these material properties is also observed in rolling processes where the components might suffer from severe so-called through-thickness inhomogeneity of texture. This results in a different crystallographic texture from the surface to the bulk due to frictions and residual stresses during rolling [2]. Similarly, during the fabrication of composites, each step of manufacturing

* Corresponding author.
E-mail address: antoine.jerusalem@eng.ox.ac.uk (A. Jérusalem).

https://doi.org/10.1016/j.cma.2022.115044

(forming, consolidation/impregnation and curing) introduces variability to the subsequent manufacturing processes and eventually the resulting properties of the structure [3]. With inaccurate design, these variabilities in geometry and material properties can severely jeopardise safety by contributing to early failures. Such failures can have devastating economic, environmental and social consequences [4] and account for as much as 10% of the total investment in new structures [5]. These uncertainties are generally not directly incorporated in the modelling methods supporting the manufacturing process as these methods (e.g., the finite element method) often rely on a deterministic description of the problem at hand. Instead, to address the various uncertainties envisaged during the design process (e.g., scenarios of overloading or inaccuracy of theoretical models, materials and manufacturing), engineers have been typically making use of safety factors, essentially using materials in excess so as to ensure safety in the functioning of their products [6]. The extra raw material going into a conservative design almost invariably translates into higher energy consumption and the concomitant emission of green house gases. Optimising the interplay between safety and environmental impact has become a major concern for most manufacturing enterprises [7]; consequently, conservative designs are now increasingly challenged. It is thus of practical interest to study as efficiently as possible the effects of uncertainties by quantifying their influence on the mechanical behaviour of a given structural component.

One way to do so can be achieved by making use of the Monte Carlo (MC) method. By gathering a number of realisations of stochastic input parameters (material properties, geometry or boundary conditions), concurrent deterministic analyses are performed for each of these realisations. The output values of interest can then be post-processed to extract their corresponding statistics (mean value, standard deviation, skewness, etc.). However, the convergence rate of this method is in $O(N^{-0.5})$, making it quickly intractable if a high fidelity system needs to be solved [8]. To this end, computationally cheaper alternative methods have been proposed. In particular, polynomial chaos expansion (PCE) was introduced by Weiner [9] and pioneered by Ghanem and Spanos [10] in the field of solid mechanics. In this method, uncertainty of both outputs and inputs are expanded using spectral representations involving orthogonal polynomials. The expression of these polynomials is determined based on an Askey scheme [11]. Strategies to obtain the unknown coefficients of these polynomials can be divided into two types. The first type, non intrusive, requires running simulations at given quadrature points [12,13] in the probability space. This method is sampling dependent, which might lead to robustness issues [14]. The second type, intrusive, performs a Galerkin projection on the stochastic dimension to obtain the unknown coefficients of these polynomials [15,16], the so-called Galerkin stochastic finite element method (GSFEM). This intrusive approach modifies the governing equation, making it difficult to use with commercial solvers.

Barring a few exceptions, the application of GSFEM to nonlinear problems remains, furthermore, relatively unexplored [17]. Nouy et al. [18] modified the extended finite element method [19] to simulate the propagation of cracks in random geometries by making use of the level-set method. The GSFEM has also been used to quantify the impact of randomness in microstructure properties on the microscopic failure probability of a composite material with unidirectional fibres using a homogenisation process [20]. Zhu et al. [21] used a stochastic multiscale analysis to study the impact of randomly oriented and aligned carbon nanotubes on the representative elementary volume size. Pivovarov and Steinman [22] also studied the influence of the randomness of the position of inclusions in composites by modelling the matrix–inclusion interface at the representative volume element level as a jump in the elastic properties of the medium described in terms of a random level-set function. As the results exhibited the Runge's phenomenon with the PCE basis, a trigonometric basis was used instead for more accurate modelling. Nair et al. [23] used MC and an interpolation scheme using an equi-probable node distribution to capture the response surface of a model exhibiting subcritical bifurcations. Though this provided a good ratio between accuracy and computational time, this method is still sampling dependent and may require a large number of simulations. Using surrogates involving continuous expansion to capture these distributions is unsuitable [24] and eventually leads to the Gibbs phenomenon [25]. Instead, Le Maitre [26] used Haar and wavelet expansions to capture the chaotic behaviour of a Lorenz system. However, to the best of our knowledge, none of these expansions have ever been used in any GSFEM framework.

Here, we propose an intrusive flexible GSFEM framework able to capture nonlinear finite deformation problems by making use of (i) a wavelet interpolation scheme for simultaneous treatment of continuous and discontinuous problems, and (ii) a modular library of stochastic operations allowing for the straightforward adaptation of any constitutive model. This approach is first validated against a 3D hyperelastic buckling problem where the distribution of the outputs exhibits sharp dependencies with respect to the distribution of the input; a problem for which

obtaining the output distributions with a direct MC approach can be inadequate if the deterministic problem is already time consuming [15,27]. We show that the proposed GSFEM implementation captures both the continuous and discontinuous aspects of the outputs in one unique simulation for a fraction of the cost of a MC approach. The methodology is then used for a problem whereby one wants to evaluate the uncertainty in the displacement of a given point within a given structure as a function of how much of the external accessible structural deformation is known. All the basic operations on probabilistic distributions (addition, multiplication and division) are performed in a custom C++ library provided as Supplementary Materials.

2. Mathematical model

This section provides the mathematical foundation for the GSFEM, details the different interpolants being used, the associated distributions and a method to adapt the approach to non-trivial custom distributions.

2.1. Stochastic space discretisation

The overarching principle of the GSFEM is to decompose any given stochastic quantity on a given space generated by a set of interpolants Ψ_ϵ. Accordingly, displacements are characterised by nodal and stochastic components, and the finite element displacement function $\boldsymbol{u}$ is written as follows:

$$\boldsymbol{u}(\boldsymbol{x},\boldsymbol{\theta}) = \sum_a N_a(\boldsymbol{x})\boldsymbol{u}^a = \sum_a N_a(\boldsymbol{x}) \sum_\epsilon \Psi_\epsilon(\theta)\boldsymbol{u}^{a\epsilon}, \tag{1}$$

where the functions N_a are the usual finite element shape functions, Ψ_ϵ the shape functions associated to the stochastic space and $\boldsymbol{u}^{a\epsilon}$ the displacement of node a with stochastic "direction" ϵ.[1] The dependence on θ denotes a function on the probability space. Consequently at a given node, both spatial and stochastic components of the displacement have to be determined. The choice of the shape functions depends on the probabilistic distribution of the inputs. For instance, if the inputs follow a Gaussian distribution, the functions Ψ_ϵ are chosen to be Hermite polynomials to ensure optimal convergence [11,28]. The deformation gradient tensor $\boldsymbol{F}$ in this stochastic finite element space follows then from the following expression:

$$\boldsymbol{F} = \sum_\epsilon \Psi_\epsilon \boldsymbol{F}^\epsilon \tag{2}$$

where, in the indicial notation, and with $\boldsymbol{\delta}$ being the Kronecker delta,

$$F^\epsilon_{iJ} = \delta_{\epsilon 1}\delta_{iJ} + \sum_a N_{a,J} u_i^{a\epsilon} \tag{3}$$

is the stochastic component of $\boldsymbol{F}$ associated with the polynomial Ψ_ϵ. Note that the presence of the identity tensor (δ_{iJ}) existing only when $\epsilon = 1$ arises from the fact that this tensor is deterministic, and that, thus, it only appears in the first term of the stochastic polynomial interpolation. Similarly, the usual finite element tensors such as the Green–Lagrange strain tensor $\boldsymbol{E}$, the first and second Piola–Kirchhoff stress tensors $\boldsymbol{P}$ and $\boldsymbol{S}$, among others, are all defined in the stochastic space.

2.2. Balance of linear momentum

In GSFEM, the equation of the balance of linear momentum with respect to the reference (or undeformed) configuration follows the same equation as its deterministic counterpart, but with the stochastic tensors, i.e.,

$$\text{Div}\, \boldsymbol{P} + \rho_0 \boldsymbol{b} = \rho_0 \ddot{\boldsymbol{u}}\,, \quad \forall \boldsymbol{X} \in \Omega_0 \ \text{ almost surely.} \tag{4}$$

where $\boldsymbol{P}$, $\boldsymbol{b}$ and ρ_0 are the stochastic first Piola–Kirchhoff stress tensor, the stochastic body force vector per unit reference mass and the stochastic reference material density.

[1] Here and subsequently, indices noted with Greek letters relate to the stochastic space.

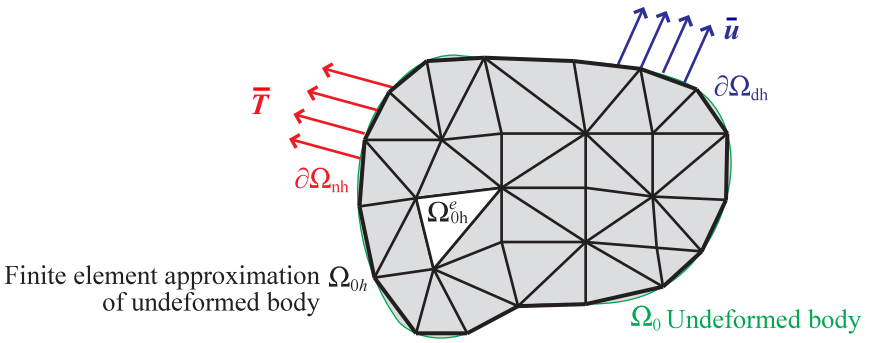

Fig. 1. Finite element discretisation of the undeformed body Ω_0 into elements Ω^e_{0h}.

2.3. Boundary conditions

Similarly, the Neumann and Dirichlet boundary conditions, $\bar{\boldsymbol{T}}$ on $\partial\Omega_n$ and $\bar{\boldsymbol{u}}$ on $\partial\Omega_d$, respectively (both potentially stochastic in nature), are imposed in the reference configuration with:

$$\begin{cases} \boldsymbol{P}\cdot\boldsymbol{N} = \bar{\boldsymbol{T}},\ \forall \boldsymbol{X}\in\partial\Omega_n \quad \text{almost surely} \\ \boldsymbol{u} = \bar{\boldsymbol{u}},\ \forall \boldsymbol{X}\in\partial\Omega_d \quad \text{almost surely,} \end{cases} \tag{5}$$

where $\boldsymbol{N}$ is the normal to the boundary in the reference configuration, and where the subscript "0" (indicating the reference configuration) of $\partial\Omega_n$ and $\partial\Omega_d$ was dropped for clarity. The body Ω_0 is discretised into elements Ω^e_{0h} such that $\Omega_{0h} = \bigcup_e \Omega^e_{0h}$, see Fig. 1.

2.4. Weak form of the balance of momentum

Let us consider a stochastic process θ in the probability space $(\Theta, \text{A}, \Gamma)$ with space of events Θ (that can be unbounded), σ-algebra A and probability measure Γ. The weak form of the balance of linear momentum described in Eq. (4) can be formulated as follows: for all arbitrary admissible virtual stochastic displacement $\boldsymbol{\eta}$, with $\boldsymbol{\eta}(\boldsymbol{X},\theta)=\boldsymbol{0}$ almost surely for all $\boldsymbol{X}\in\partial\Omega_d$,

$$\int_\Theta\int_{\Omega_0} \text{Div}\,\boldsymbol{P}\cdot\boldsymbol{\eta}\,\text{d}V\text{d}\Gamma(\theta) + \int_\Theta\int_{\Omega_0}\rho_0\boldsymbol{b}\cdot\boldsymbol{\eta}\,\text{d}V\text{d}\Gamma(\theta) = \int_\Theta\int_{\Omega_0}\rho_0\ddot{\boldsymbol{u}}\cdot\boldsymbol{\eta}\,\text{d}V\text{d}\Gamma(\theta). \tag{6}$$

Note the second integral over the stochastic space Θ. Integrating by parts and using Green's theorem, the above expression can be rewritten as

$$\int_\Theta\int_{\partial\Omega_0}(\boldsymbol{P}\cdot\boldsymbol{N})\cdot\boldsymbol{\eta}\,\text{d}S\text{d}\Gamma(\theta)+\int_\Theta\int_{\Omega_0}\rho_0\boldsymbol{b}\cdot\boldsymbol{\eta}\,\text{d}V\text{d}\Gamma(\theta) = \int_\Theta\int_{\Omega_0}\boldsymbol{P}:\text{Grad}\,\boldsymbol{\eta}\,\text{d}V\text{d}\Gamma(\theta)+\int_\Theta\int_{\Omega_0}\rho_0\ddot{\boldsymbol{u}}\cdot\boldsymbol{\eta}\,\text{d}V\text{d}\Gamma(\theta), \tag{7}$$

which, noting that $\boldsymbol{\eta}=\boldsymbol{0}$ almost surely for all $\boldsymbol{X}\in\partial\Omega_d$ and using Eq. (5), leads to

$$\int_\Theta\int_{\partial\Omega_n}\bar{\boldsymbol{T}}\cdot\boldsymbol{\eta}\,\text{d}S\text{d}\Gamma(\theta)+\int_\Theta\int_{\Omega_0}\rho_0\boldsymbol{b}\cdot\boldsymbol{\eta}\,\text{d}V\text{d}\Gamma(\theta) = \int_\Theta\int_{\Omega_0}\boldsymbol{P}:\text{Grad}\,\boldsymbol{\eta}\,\text{d}V\text{d}\Gamma(\theta)+\int_\Theta\int_{\Omega_0}\rho_0\ddot{\boldsymbol{u}}\cdot\boldsymbol{\eta}\,\text{d}V\text{d}\Gamma(\theta). \tag{8}$$

The relation between $\boldsymbol{P}$ and $\boldsymbol{F}$ is defined by the material constitutive law $\boldsymbol{P}=\tilde{\boldsymbol{P}}(\boldsymbol{F})$.

2.5. Numerical integration

Both displacements (real and virtual) and stresses are now stochastic quantities. The same decomposition as in Eq. (1) applies for all other stochastic quantities with the stochastic shape functions Ψ_ϵ being space independent.

GSFEM problem: Find all $\boldsymbol{u}^a \in \mathbb{R}^3 \times \Theta$ such that for all admissible virtual displacement $\boldsymbol{\eta}^b \in \mathbb{R}^3 \times \Theta$:

$$\begin{aligned}\sum_e \int_\Theta \int_{\Omega_0^e} \rho_0^\kappa N_a^e N_b^e \ddot{\boldsymbol{u}}^{a\epsilon} \cdot \boldsymbol{\eta}^{b\iota}\, \Psi_\kappa\, \Psi_\epsilon\, \Psi_\iota \,\mathrm{d}V \mathrm{d}\Gamma(\theta) + \sum_e \int_\Theta \int_{\Omega_0^e} \left(\tilde{\boldsymbol{P}}\,(\boldsymbol{F}) \cdot \nabla_0 N_b^e\right) \cdot \boldsymbol{\eta}^{b\iota}\, \Psi_\iota \,\mathrm{d}V \mathrm{d}\Gamma(\theta) \\ = \sum_e \int_\Theta \int_{\partial\Omega_n^e} N_b^e \bar{\boldsymbol{T}} \cdot \boldsymbol{\eta}^{b\iota}\, \Psi_\iota \,\mathrm{d}S \mathrm{d}\Gamma(\theta) + \sum_e \int_\Theta \int_{\Omega_0^e} \rho_0^\kappa N_b^e \boldsymbol{b} \cdot \boldsymbol{\eta}^{b\iota}\, \Psi_\kappa\, \Psi_\iota \,\mathrm{d}V \mathrm{d}\Gamma(\theta).\end{aligned} \tag{9}$$

Since the above equation must be valid for all admissible $\boldsymbol{\eta}^b$, the finite element problem now reads: Find $\boldsymbol{u}^a$ such that, for all b,

$$\sum_e M^e_{\epsilon b\iota a} \ddot{\boldsymbol{u}}^{a\epsilon} + \sum_e \boldsymbol{f}^{e\,\mathrm{int}}_{\iota b} = \sum_e \boldsymbol{f}^{e\,\mathrm{ext}}_{\iota b}, \tag{10}$$

where the stochastic mass tensor $\boldsymbol{M}^e$, the stochastic element internal force vector $\boldsymbol{f}^{e\,\mathrm{int}}$ and the stochastic external force vector $\boldsymbol{f}^{e\,\mathrm{ext}}$ are

$$M^e_{\epsilon b\iota a} = \int_\Theta \int_{\Omega_0^e} \rho_0^\kappa N_a^e N_b^e\, \Psi_\kappa\, \Psi_\epsilon\, \Psi_\iota \,\mathrm{d}V \mathrm{d}\Gamma(\theta), \tag{11}$$

$$\boldsymbol{f}^{e\,\mathrm{int}}_{\iota b} = \int_\Theta \int_{\Omega_0^e} \tilde{\boldsymbol{P}}\,(\boldsymbol{F}) \cdot \nabla_0 N_b^e\, \Psi_\iota \,\mathrm{d}V \mathrm{d}\Gamma(\theta), \tag{12}$$

$$\boldsymbol{f}^{e\,\mathrm{ext}}_{\iota b} = \int_\Theta \int_{\partial\Omega_n^e} N_b^e \bar{\boldsymbol{T}}\, \Psi_\iota \,\mathrm{d}S \mathrm{d}\Gamma(\theta) + \int_\Theta \int_{\Omega_0^e} \rho_0^\kappa N_b^e \boldsymbol{b}\, \Psi_\kappa\, \Psi_\iota \,\mathrm{d}V \mathrm{d}\Gamma(\theta). \tag{13}$$

After expanding $\tilde{\boldsymbol{P}}$ as $\tilde{\boldsymbol{P}}^\tau\, \Psi_\tau$, $\bar{\boldsymbol{T}}$ and $\boldsymbol{b}$ in the same manner, the internal and external forces vectors become:

$$\boldsymbol{f}^{e\,\mathrm{int}}_{\iota b} = \int_\Theta \int_{\Omega_0^e} \tilde{\boldsymbol{P}}^\tau \cdot \nabla_0 N_b^e\, \Psi_\iota\, \Psi_\tau \,\mathrm{d}V \mathrm{d}\Gamma(\theta), \tag{14}$$

$$\boldsymbol{f}^{e\,\mathrm{ext}}_{\iota b} = \int_\Theta \int_{\partial\Omega_n^e} N_b^e \bar{\boldsymbol{T}}_\tau\, \Psi_\iota\, \Psi_\tau \,\mathrm{d}S \mathrm{d}\theta + \int_\Theta \int_{\Omega_0^e} \rho_0^\kappa N_b^e \boldsymbol{b}_\tau\, \Psi_\kappa\, \Psi_\iota\, \Psi_\tau \,\mathrm{d}V \mathrm{d}\Gamma(\theta). \tag{15}$$

For simplification purposes, the quantity $\int_\Theta f(\theta) g(\theta) \mathrm{d}\Gamma(\theta)$ is noted $\langle f, g \rangle$ where f and g are two stochastic functions. As, by virtue of orthogonality, $\langle \Psi_\iota,\, \Psi_\tau \rangle$ is different from zero only when $\iota = \tau$, the force vectors can be further simplified by:

$$\boldsymbol{f}^{e\,\mathrm{int}}_{\iota b} = \int_{\Omega_0^e} \tilde{\boldsymbol{P}}^\iota \cdot \nabla_0 N_b^e \langle \Psi_\iota,\, \Psi_\iota \rangle \,\mathrm{d}V \tag{16}$$

$$\boldsymbol{f}^{e\,\mathrm{ext}}_{\iota b} = \int_{\partial\Omega_n^e} N_b^e \bar{\boldsymbol{T}}_\tau \langle \Psi_\iota,\, \Psi_\iota \rangle \,\mathrm{d}S + \int_{\Omega_0^e} \rho_0^\kappa N_b^e \boldsymbol{b}_\iota \langle \Psi_\kappa\, \Psi_\iota,\, \Psi_\tau \rangle \,\mathrm{d}V. \tag{17}$$

Using Gauss quadrature, one then has:

$$M^e_{\iota a\epsilon b} = \sum_q w_q \rho_0^\kappa N_a^e(\boldsymbol{\xi}_q) N_b^e(\boldsymbol{\xi}_q) J_0(\boldsymbol{\xi}_q) \langle \Psi_\kappa\, \Psi_\epsilon,\, \Psi_\iota \rangle, \tag{18}$$

$$f^{e\,\mathrm{int}}_{\iota ia} = \sum_q w_q P^\iota_{iJ}(\boldsymbol{\xi}_q) N^e_{a,J}(\boldsymbol{\xi}_q) J_0(\boldsymbol{\xi}_q) \langle \Psi_\iota,\, \Psi_\iota \rangle, \tag{19}$$

$$f^{e\,\mathrm{ext}}_{\iota ib} = \sum_p w_p T^\iota_i(\boldsymbol{\xi}_p) N_b^e(\boldsymbol{\xi}_p) J_0(\boldsymbol{\xi}_p) \langle \Psi_\iota,\, \Psi_\iota \rangle + \sum_q w_q \rho_0^\kappa b_{\iota i}(\boldsymbol{\xi}_q) N_b^e(\boldsymbol{\xi}_q) J_0(\boldsymbol{\xi}_q) \langle \Psi_\kappa\, \Psi_\epsilon,\, \Psi_\iota \rangle. \tag{20}$$

where $\boldsymbol{\xi}_q$ is the coordinate vector of Gauss point q (of element e) in the isoparametric coordinate system, w_q is its corresponding weight, and J_0 is the Jacobian between the isoparametric coordinate system and the reference configuration. The term with the sum in p (first term of Eq. (20)) is on the surface elements belonging to $\partial\Omega^e_{dh}$ mapped onto the corresponding faces of the volume elements. Note that this quadrature only concerns the physical space as all integrals on the stochastic space can be computed without any numerical approximations.

As the internal force vector $\boldsymbol{f}^{e\,\mathrm{int}}$ is not necessarily linear, a Newton–Raphson procedure can be used to enforce Eq. (10). In this case, the stochastic element stiffness matrix $\boldsymbol{K}^e$ is needed:

$$R^e_{ia} = f^{e\,\mathrm{int}}_{ia} - f^{e\,\mathrm{ext}}_{ia}, \tag{21}$$

$$K^e_{ia\epsilon kb} = \frac{\partial R^e_{ia}}{\partial u_{\epsilon kb}} = \frac{\partial f^{e\,\mathrm{int}}_{ia}}{\partial u_{\epsilon kb}} = \sum_q w_q \frac{\partial P^i_{iJ}}{\partial F^\omega_{qM}} \frac{\partial F^\omega_{qM}}{\partial u_{\epsilon kb}} (\boldsymbol{\xi}_q) N^e_{a,J}(\boldsymbol{\xi}_q) J_0(\boldsymbol{\xi}_q), \tag{22}$$

where R is the stochastic residual vector and where

$$\frac{\partial F^\omega_{qM}}{\partial u_{\epsilon kb}} = \delta_{qk} N_{b,M} \delta_{\epsilon\omega}. \tag{23}$$

Note that the external force vector is assumed here to be deformation independent for simplicity, but this term could be added straightforwardly if needed (e.g., when a pressure on the deformed surface is imposed or gravity is needed).

2.6. Constitutive model

The function $\boldsymbol{P} = \tilde{\boldsymbol{P}}(\boldsymbol{F})$ and its derivative (the stochastic tangent modulus) are provided by the constitutive law. When using GSFEM, theirs numerical expressions are not straightforward as stochastic quantities are involved. They can, however, be facilitated by the use of stochastic operator mirroring their deterministic counterparts, see Appendix A.1. Doing so in the case of the hyperelastic Saint Venant–Kirchhoff model used in Section 4 means that the formulation of the stochastic second Piola–Kirchhoff stress tensor $\boldsymbol{S}$ can be linked to the stochastic Green–Lagrange strain tensor $\boldsymbol{E}$ by

$$\boldsymbol{S} = 2\mu \hat{\times} \boldsymbol{E} \hat{+} \lambda \hat{\times} \hat{tr}(\boldsymbol{E}), \tag{24}$$

where $\boldsymbol{P} = \boldsymbol{F} \hat{\cdot} \boldsymbol{S}$ and $\boldsymbol{E} = 1/2(\boldsymbol{F}^T \hat{\cdot} \boldsymbol{F} \hat{+} \boldsymbol{I})$. See Appendix A.1 for the definition of the operators $\hat{\times}$, $\hat{+}$, $\hat{tr}$ and $\hat{\cdot}$. Here, λ and μ are stochastic Lamé constants.

The complete derivation of the tangent modulus for the Saint Venant–Kirchhoff model is provided in Appendix A.2. Other material models can be easily developed using the provided stochastic operator toolbox, provided as a C++ library in Supplementary Material.

2.7. Expansion of the solution

This section details the three polynomial expansions used in this work: polynomial chaos, Haar and wavelet.

2.7.1. Polynomial chaos expansion

The PCE, introduced for first time by Weiner [9], was aimed at creating a metamodel that determines the evolution of uncertainty in a dynamical system. This metamodel is dependent on the probabilistic distribution of input parameters. According to the Cameron–Martin theorem [28], such an expansion converges in the L_2 sense for a stochastic process with finite variance depending on Gaussian stochastic variables. Xiu and Karniadakis [11] extended these results to various probabilistic distribution of the inputs. The PCE interpolant univariate polynomials $\psi_\lambda(\theta)$, where λ is the degree of the polynomial, must verify this integral:

$$\int_\Omega \psi_\lambda(\theta)\psi_{\lambda'}(\theta) f(\theta) d\theta = 0 \text{ if } \lambda \neq \lambda', \tag{25}$$

where the function $f(\theta)$ is the probability distribution of the stochastic variable θ. The polynomials ψ's are determined recursively and depend on the distribution of θ; for instance, they are Hermite polynomials if θ follows a Gaussian distribution, and Legendre polynomials for a uniform distribution [11]. Uniqueness of these polynomials is imposed by setting the coefficient of the highest degree to 1.

Let us now consider $\boldsymbol{\theta} = [\theta_1, \ldots, \theta_N]$ a vector of random variables [10] defined in the space $\Theta_1 \times \cdots \times \Theta_N$. For simplicity, the stochastic variables are supposed to be uncorrelated so that the joint probabilistic distribution is

the product of each probabilistic distribution functions [11]. The M multivariate polynomials Ψ's of the PCE on $\Theta_1 \times \cdots \times \Theta_N$ are defined as follows:

$$\Psi \in \left\{ \prod_{i=1}^{N} \psi_{\lambda_i}(\theta_i) : \sum_{i=0}^{N} \lambda_i \leq n \right\}, \tag{26}$$

where λ_i refers to the order of the univariate polynomial associated to θ_i and where n indicates the degree of the expansion. The number of multivariate polynomials in a PCE expansion of order n is $M = \binom{n+N}{n}$. These expansions are suitable when the quantity of interest exhibits a smooth dependence on the input parameters.

2.7.2. Haar expansion

The use of PCE can sometime lead to instabilities such as the Gibbs phenomenon (see Section 4). To overcome this limitation of the PCE expansion, the stochastic inputs and the solution can be decomposed instead using Haar expansion [29]. Given a stochastic variable θ, we note $p(x)$ the probability that $\theta < x$, where x is a real number. The function p is assumed to be a continuous strictly increasing function of x. Based on these assumptions, there is one unique solution x such that $p(x) = y$, where $0 \leq y \leq 1$. We note $F = p^{-1}$ and we introduce the Haar function ψ^h:

$$\psi^h(y) = \begin{cases} 1, & \text{if } 0 \leq y \leq 0.5 \\ -1, & \text{if } 0.5 \leq y \leq 1 \\ 0, & \text{otherwise.} \end{cases}$$

The Haar function is the mother wavelet that generates the wavelet family:

$$\psi_{j,k}(y) = 2^{\frac{j}{2}} \psi^h(2^j y - k), \tag{27}$$

where $j = 0, \ldots, n$ is the scale index and $k = 0, \ldots, 2^j - 1$ is the space index, with n being a user-defined index indicating the resolution of the expansion. Any stochastic process X function of the stochastic variable θ with finite variance can be approximated arbitrary well by the following expression:

$$X = \bar{X} + \sum_{j=0}^{n} \sum_{k=0}^{2^j - 1} X_{j,k} \psi_{j,k}. \tag{28}$$

The values of $X_{j,k}$ are determined by a scalar projection of X on the functions $\Psi_{j,k}$:

$$X_{j,k} = \int_0^1 X\left(F(y)\right) \psi_{j,k}(y) dy. \tag{29}$$

For the sake of simplicity, we concatenate the two indices j and k using an integer $\lambda = 2^k + j$. We note ∇ the set of integers λ, $\nabla \equiv \{\lambda : j = 0, \ldots, n, k = 2^j - 1\}$. Noting $\psi_0 = 1$, and $\nabla_0 = \nabla \cup \{0\}$, Eq. (28) can be rewritten as:

$$X = \sum_{\lambda \in \nabla_0} X_\lambda \psi_\lambda. \tag{30}$$

Considering now a multi-dimensional stochastic process, with multi-dimensional index $\boldsymbol{\lambda} = [\lambda_1, \ldots, \lambda_N]$ the univariate sequence defined by Eq. (27) is used to create the multivariate family Ψ^H:

$$\Psi^H = \left\{ \prod_{k=1}^{N} \psi_{\lambda_k}(\theta_k) : \sum_{k=1}^{N} |\lambda_k| \leq n \right\}, \tag{31}$$

where n is the level of resolution.

2.7.3. Wavelet expansion

The Haar expansion, while allowing to capture discontinuous behaviours, can require a high level of resolution to capture continuous distributions, see Section 4. To overcome this issue, we propose here to use the so-called wavelet expansion. The wavelet expansion uses both continuous and discontinuous functions. Here, a space V^N, containing polynomials of order equal or smaller than N is constructed with a cardinality of $N + 1$. Typically, the scaled Legendre polynomials $[\phi_0, \ldots, \phi_{N+1}]$ are used as a basis of V^N. Discontinuous orthonormal functions $[\psi_0, \ldots, \psi_N]$ are then built as follows [30]:

Table 1
Correspondence of the type of polynomial chaos and the underlying probabilistic distribution of the input.

Input probabilistic distribution	Polynomial chaos
Gaussian	Hermite
Uniform	Legendre
Gamma	Laguerre
Beta	Jacobi

(i) Two sets of polynomials $p_i(y)$ and $q_i(y)$ are defined:

$$\begin{cases} p_i(y) = y^i \\ q_i(y) = \begin{cases} p_i(y), & \text{if } 0 \leq y \leq 0.5 \\ -p_i(y), & \text{if } 0.5 < y \leq 1. \end{cases} \end{cases}$$

(ii) Each polynomial q_i is orthogonalised with respect to the functions p_i to obtain a new set of polynomials $[\tilde{q}_0, \ldots, \tilde{q}_{N+1}]$;
(iii) Using a Gram–Schmidt scheme, the set of polynomials $[\tilde{q}_0, \ldots, \tilde{q}_{N+1}]$ are orthogonalised with respect to each other to give a set of polynomials $[r_0, \ldots, r_{N+1}]$;
(iv) The set of polynomials $[r_0, \ldots, r_{N+1}]$ is normalised to obtain the functions $[\psi_0, \ldots, \psi_{N+1}]$.

Note that, by construction, the functions ψ_i and ϕ_j are orthogonal. We then define the functions ψ_{ik}^j as:

$$\psi_{ik}^j(y) = 2^{\frac{j}{2}} \psi_i(2^j y - k). \tag{32}$$

Similarly to Eq. (28), a given stochastic process is finally expanded using the wavelet expansion:

$$X(y) = \sum_{i=0}^{N} X_i \phi_i(y) + \sum_{i=0}^{N} \sum_{j=0}^{n} \sum_{k=0}^{2^j-1} X_{i+(N+1)(2^j+k)} \psi_{il}^k(y). \tag{33}$$

The coordinates X_i of a stochastic process X, where $i = 0, \ldots, 2^{n+1}(N+1) - 1$, are obtained by projection on the functions ψ_i and ϕ_i. More information can be found about the underlying mathematical theory of these expansions in Ref. [30] and [26].

2.8. Uncertainty of the inputs

The GSFEM and its underlying mathematical theory suppose full knowledge of the probability distribution of the input variables. These distributions are often idealised by researchers for ease of manipulation or when data are not available. While doing so allows for more flexibility, e.g., the computation of the univariate polynomial chaos with closed forms, more realistic distributions can be found using experimental data and/or Bayesian inference, potentially better capturing the uncertainties. In the following, we propose a method for each one of the two approaches.

2.8.1. Idealised input distributions

Gaussian distributions have been widely used in the research community to model the uncertainties of material properties [12,13,31]. Taking into account the fact that many observable phenomena result from the superposition of smaller stochastic perturbations, these distributions are ubiquitous in nature as a consequence of the central limit theorem [32]. Using these distributions proves to be highly practical to build the expansions defined in Section 2.7. The corresponding PCE for usual distributions are given in Table 1. The closed form of the PCE using Gaussian variables and some insights on the construction of the discontinuous expansions are also provided in more detail in Appendix A.3. Note that the continuous and discontinuous expansions presented in Section 2.7 can still be used for more complex and realistic distributions, given additional effort.

2.8.2. User-provided input distributions

To improve the accuracy of stochastic simulations, the distributions of the input variables can be determined through experimental data. For example, researchers have been using Bayesian inference for the identification of space-independent elastoplastic material parameters [33]. The proposed framework offers a way to include such measured distributions. The only step that has to be modified is the one where the expansions are built. In general cases, finding a closed form of these expansions is impossible. Consequently, Eq. (25) has to be enforced numerically in order to find the associated polynomial expansion. When building Haar and wavelet expansions, only the knowledge of the joint probability distributions and the cumulative distributions of the inputs variables is required. In the case where one of the inputs is a given stochastic field $P(\boldsymbol{x}, \boldsymbol{\theta})$ with a spatial correlation $C(\boldsymbol{x}_1, \boldsymbol{x}_2)$, it is possible to decompose P using the Karhunen–Loève theorem [34]:

$$P(\boldsymbol{x}, \boldsymbol{\theta}) = \bar{P}(\boldsymbol{x}) + \sum_{i=1}^{\infty} \sqrt{\lambda_i}\, f_i(\boldsymbol{x}) \epsilon_i(\boldsymbol{\theta}), \tag{34}$$

where $\epsilon_i(\boldsymbol{\theta})$ has a null mean and standard deviation of 1 and $\bar{P}(\boldsymbol{x})$ is the mean value of $P(\boldsymbol{x}, \boldsymbol{\theta})$. λ_i and f_i are respectively called eigenvalues and eigenfunctions. f_i are pairwise orthogonal in $L_2([a, b])$. They must be the solution of the Fredholm equation [35]:

$$\int_D C(\boldsymbol{x}_1, \boldsymbol{x}_2) f_i(\boldsymbol{x}_1) d\boldsymbol{x}_1 = \lambda_i f_i(\boldsymbol{x}_2). \tag{35}$$

However, the determination of the functions $\epsilon_i(\boldsymbol{\theta})$ requires performing an iterative process, see Ref. [36] for more detail. While the code used for the following simulations does not yet include random field properties capabilities, the definition of the λ_i and f_i as a preprocessing step for a given problem readily allows a straightforward implementation.

3. Modularity of the code

In GSFEM, solving both the stochastic and spatial finite element problem at the same time requires the modification of the governing equations. As such, using a commercial solver is impractical. However, with appropriate changes, an in-house finite element code can be modified intrusively to perform simulations of stochastic problems. The general framework of any finite element software can be summarised as shown in Fig. 2. At first, an input file gathering all the information about the geometry, connectivity, type of simulation, constitutive model, value of parameters, etc., has to be read. Subsequently, and at each iteration, the displacements are updated either explicitly or implicitly to satisfy the mechanical equilibrium. The time of the simulation is then advanced and the process is repeated, until the end time is reached. Finally, the outputs are post-processed (or once in a while during the course of the simulation).

In Fig. 2, the parts of the solver that require modifications are specified in lighter green. The writing and reading of the input file has to be done so that the probabilistic distributions of each stochastic variable (geometry, constitutive parameters, initial conditions) are specified. Before the computation of internal/external forces, key mathematical quantities, such as the third order tensor $\boldsymbol{C}$, see Appendix A.1, are computed once and for all and stored for computational efficiency. The computation of the internal, external inertial forces and stiffness matrices are modified accordingly. These modifications can be done in a modular way using a stochastic algebra library. This algebra allows for the computation of basic operations such as addition/multiplication/division of stochastic variables, see also Ref. [17,37].

4. Applications

This section illustrates the methodology described above with two different stochastic problems. The first one studies the performance of three different expansions (PCE, Haar and mixed wavelet) for a beam buckling problem where the beam tip is submitted to a stochastic axial displacement. The second application idealises a problem whereby one wants to know the uncertainty in the displacement of a given point in a structure as a function of how much of the external accessible structure deformation is known.

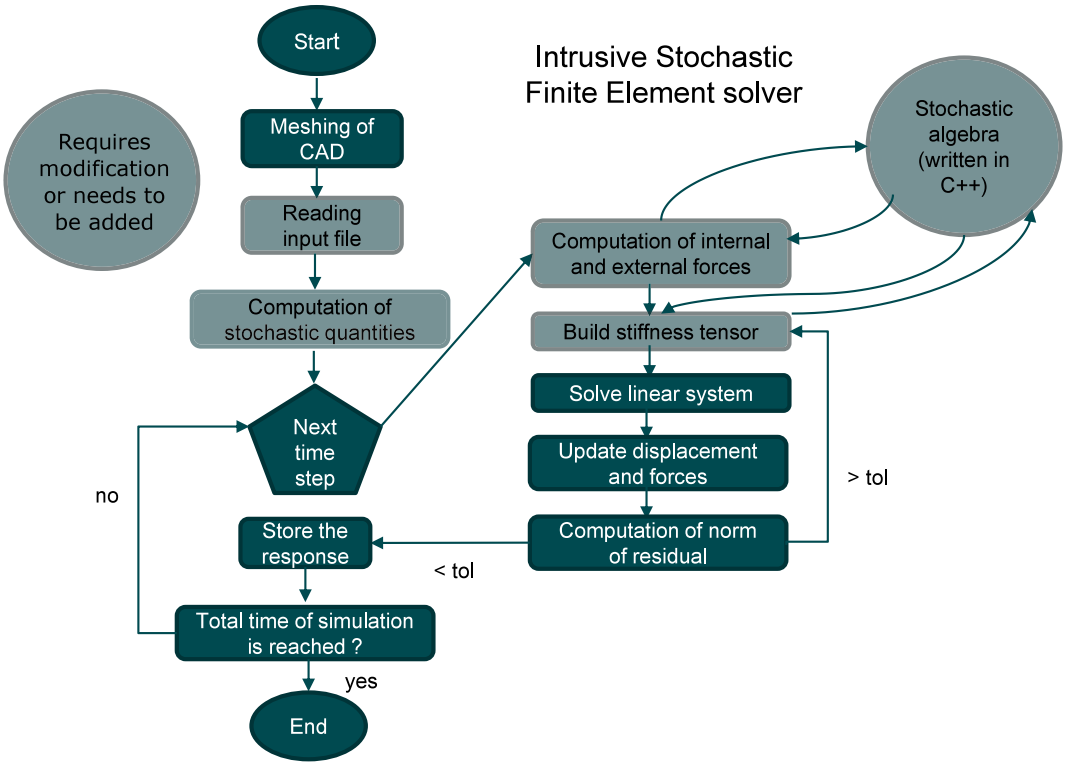

Fig. 2. Scheme of the stochastic in-house code. The differences with the deterministic solver are indicated in lighter green. (For interpretation of the references to colour in this figure legend, the reader is referred to the web version of this article.)

4.1. Stochastic buckling

Bifurcation problems is a common challenge in structural mechanics problems. In such cases, a slight variation in an input parameter can dramatically change the output values. Consequently, the distribution of outputs may exhibit discontinuous and/or sharp behaviours. Here, we idealise such problem by considering a 3D beam clamped at its left extremity and submitted to an axial displacement on its right extremity, see Fig. 3(a). If this displacement compresses the structure above a certain threshold, the beam will buckle and experience large lateral displacements at the tip (either up or down in Fig. 3(a)). However, if this displacement is tensile, then the lateral displacement of the tip should be null, or close to. Here, we prescribe an axial displacement following a Gaussian distribution centred on zero displacement, see Fig. 3(b). Boundary conditions are prescribed such that the lateral surfaces cannot move in the z-direction. To facilitate buckling and control its direction, we impose a negligible deterministic displacement in the y-direction on the tip to guide the buckling in one specific direction. Finally, the material constitutive behaviour is modelled with a Saint Venant–Kirchhoff model. The geometry of the beam, the finite element discretisation and the material properties are given in Table 2. While the proposed scheme assumes a priori that the constitutive parameters are stochastic, we restrict the stochasticity of our model to the boundary conditions described above and retain deterministic material parameters. The aim of this study is thus to provide an accurate description of a non-smooth[2] output distribution (lateral displacement of the midpoint of the tip) with respect to a continuous input distribution (prescribed axial displacement) in an effective way.

4.2. Structural deformation uncertainty estimation

Manufacturing processes invariably introduce uncertainties in the morphology and/or material properties of all components, which then manifest themselves through the existence of stress residual and some degree of randomness

[2] Here, buckling creates a lateral displacement whose function of the longitudinal displacement is not C^1.

Table 2
Geometry, FE discretisation and material parameters the beam.

Parameter	Value
Geometry (arbitrary units)	Length = 25, width = depth = 1
Number of nodes	1336
Type of elements	Quadratic tetrahedra
Number of elements	703
Mean value of axial displacement	0
Standard deviation of axial displacement	1
Young's modulus	10^7 Pa
Poisson's ratio	0.4

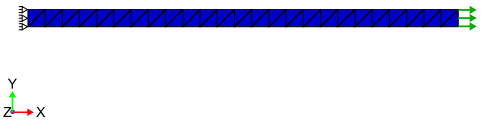

(a) Discretised FE 3D beam (side view) loading conditions: the beam is clamped on its left side and submitted to a stochastic axial displacement on the right side.

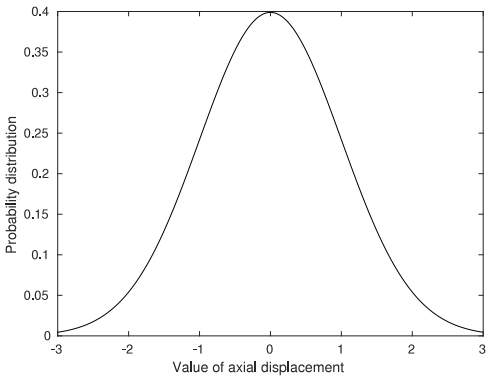

(b) Gaussian Probabilistic distribution of the axial displacement.

Fig. 3. A 3D beam is submitted to stochastic boundary conditions triggering buckling when the displacement compresses the structure.

in the deformation of the in-service manufactured structural components. Understanding the movement of one or multiple material points within a structure can then be monitored by making use of different sensors such as strain gauges. In this example, we idealise a problem whereby one wants to estimate the position of the centre of a disc when the radial displacements of the four poles N(North), E(East), S(South) and W(West) of the discs are either known exactly (chosen arbitrarily—and without loss of generality—to be a displacement of 0) or unknown within a Gaussian distribution centred on 0 for a given standard deviation, see Fig. 4. Five different simulations are performed. In the first one, a radial stochastic displacement is imposed at every cardinal point. In the second one, W is clamped, i.e., it has a known deterministic displacement equal to 0. In the third and fourth simulations, only two cardinal points, respectively, N and S, and E and S, follow a random radial displacement. In the last simulation, only the radial displacement of S is random. For each simulation, the x- and y-displacements of the centre of the disc O are evaluated. We expect the problem to be smooth enough for a PCE of degree 3 to give accurate results. The material constitutive behaviour is modelled with a plane stress Saint Venant–Kirchhoff model. The geometrical features of the disc, its finite element discretisation and the material properties are given in Table 3.

4.3. Results

A comparison between the non-intrusive approach (MC) and intrusive approach with continuous (PCE) and discontinuous expansions (Haar and wavelet) is first provided by making use of the stochastic buckling problem. All simulations are performed in our in-house code software, MuPhiSim. The results using MC provide a baseline for comparisons as this framework ensures that, given enough simulations, the output's probabilistic distribution is accurately captured. The distribution of the lateral tip displacement is shown in Fig. 5. Two regimes can be observed. When the displacement is negative enough (compressive), the lateral displacement varies quickly with the axial displacement. When the displacement is positive (tensile), the displacement does not vary with the axial displacement.

Table 3
Geometry, FE discretisation and material parameters of the disc.

Parameter	Value
Geometry (arbitrary units)	Radius = 10
Number of nodes	1393
Type of elements	Linear triangles
Number of elements	2658
Mean value of axial displacement	0
Standard deviation of radial displacement (when applied)	0.1
Young's modulus	10^6 Pa
Poisson's ratio	0.4

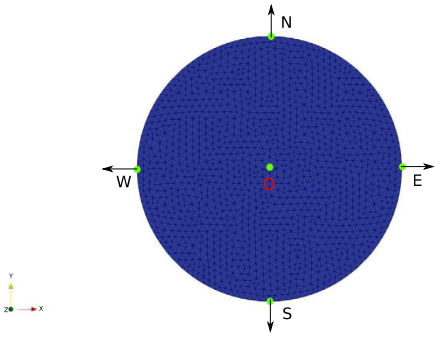

(a) Discretised FE 2D disc loading conditions: displacements are prescribed at the points N,E,S and W.

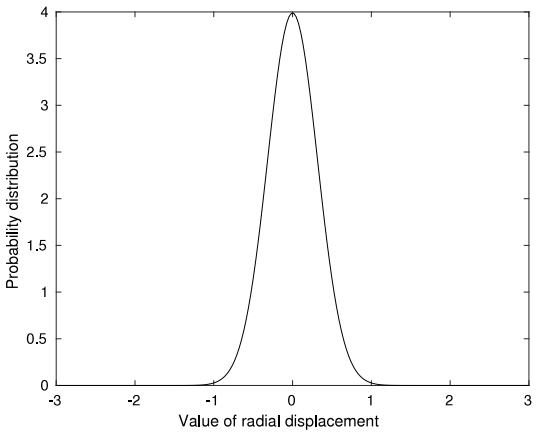

(b) Probabilistic distribution of the radial displacement. The displacement is supposed to be either random (blue histogram) or deterministic and equal to 0 (red histogram)

Fig. 4. Radial displacements are applied at the cardinal points N, E, S and W of a disc. Different configurations are studied where, at each cardinal point, the displacement is either uncertain or known and equal to 0. The distribution of the x- and y-displacements at the centre O is then evaluated.

While roughly capturing the MC results, approaching the distribution of the lateral tip displacement using PCE is ineffective, see Fig. 6(a). Indeed, increasing the order of the expansion only results in greater oscillations and does not guarantee convergence. This is predictable as using smooth functions to approximate a non-smooth function is known to lead to such issue, the so-called Gibbs phenomenon. The inaccuracy of the PCE approach can also be seen when comparing the cumulative distribution functions (CDF) of the lateral displacement, see Fig. 6(b). Despite some convergence on part of the curves, the PCE is unable to capture the sharp increase in the CDF.

When using discontinuous expansions, the results are more promising. Indeed, Fig. 7(a) shows that Haar expansions are able to capture accurately the transition between the plateau and the smooth part of the tip displacement distribution. This is expected as Haar expansions are intrinsically discontinuous. However, the convergence of these expansions is slow, see Fig. 7(b), and would require too much computational time as increasing the order by one increases the number of degree of freedom by a factor two.

The wavelet expansion mixing smooth and discontinuous expansions is giving the most accurate results with minimal numbers of degree of freedoms (we chose here the values $n = N = 1$ in Eq. (33)), and with a simulation time a factor three smaller than with the MC approach. In Fig. 8(a), both the smooth part and the plateau of the distribution are captured with precision. It can be noted that the extreme negative part of the curve is not properly captured, in line with the fact that this region belongs to the tail of the Gaussian distribution: 96% of the Gaussian distribution lies in the range $[-2,2]$. Indeed, Fig. 8(b) shows that the discrepancies at the left tail are negligible as the CDF of both wavelet approximation and MC are close when the CDF approaches unity. The information contained in approximately $\sim$1000 simulations can be obtained with only one simulation with 8 times

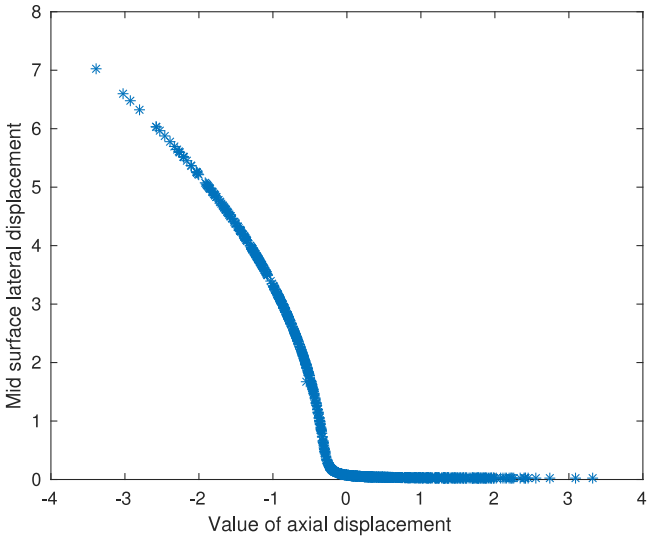

Fig. 5. Distribution of the tip displacement using the Monte Carlo method.

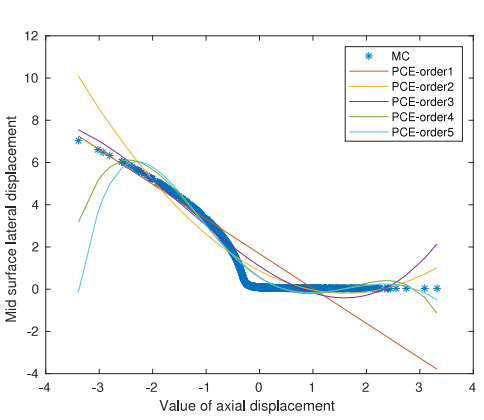

(a) Comparison of the distribution of the tip displacement using polynomial chaos expansion and Monte Carlo.

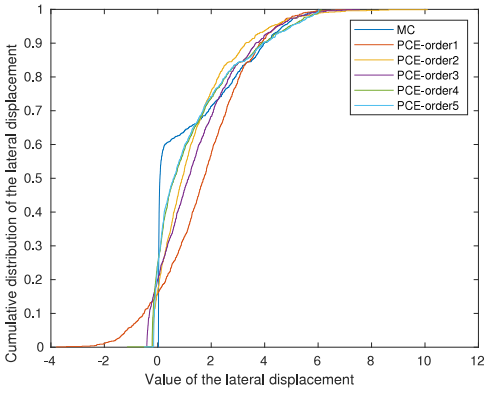

(b) Comparison of the cumulative distribution functions of the tip displacement using polynomial chaos expansion and Monte Carlo.

Fig. 6. Performance of the PCE in capturing discontinuous behaviour.

more degrees of freedoms. We recall that this increase of degrees of freedoms comes from the fact that both the spatial and stochastic finite element problems are solved at the same time. The use of the mixed wavelet method however leads to the prediction of non-physical negative values. While this certainly hampers the efficiency of the proposed method, the issue can be easily alleviated by either increasing the order of the polynomial expansion (N in Eq. (33)) or the number of discontinuities (n in Eq. (33)), though at a computational cost.

The results of the second problem demonstrates how the method allows to quantitatively evaluate how the magnitude of the uncertainties of the output decreases when boundary conditions (radial displacements at the cardinal points) are known with more precision, in an approach akin to Schrödinger's cat experiment. Fig. 9(a) shows that the distribution of the x-displacement of the centre of the circle narrows down as the degree of stochasticity in the boundary conditions decreases. Note that the probabilistic distributions of the outputs in this figure are obtained through GSFEM and not MC; the histogram representation is due to the fact that up to four independent random variables are used and, while the distributions of the x- and y-displacements are known analytically as a function of those four variables, plotting them by probability of occurrence requires using sampled values of the stochastic variables (Gaussian centred distribution in this case), taken to 100,000 samples here (a 5D plot would be required

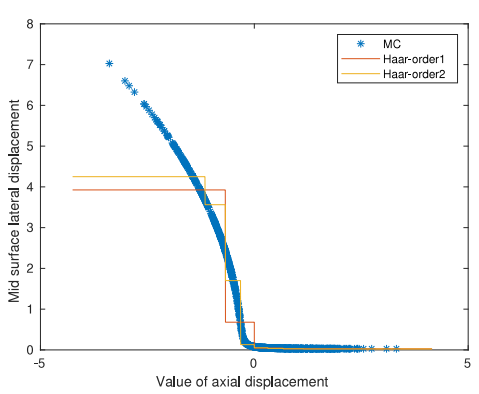

(a) Comparison of the distribution of the tip displacement using Haar expansion and Monte Carlo.

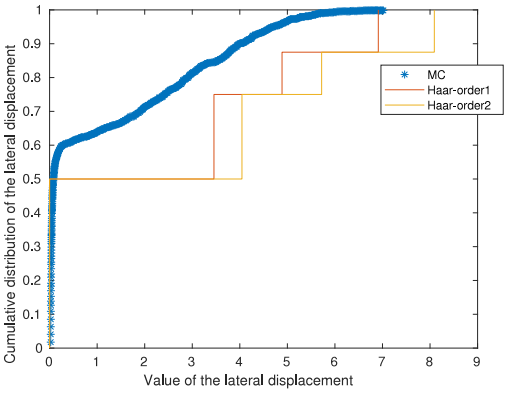

(b) Comparison of the cumulative distribution functions of the tip displacement using Haar expansion and Monte Carlo.

Fig. 7. Performance of the Haar polynomials in capturing discontinuous behaviour.

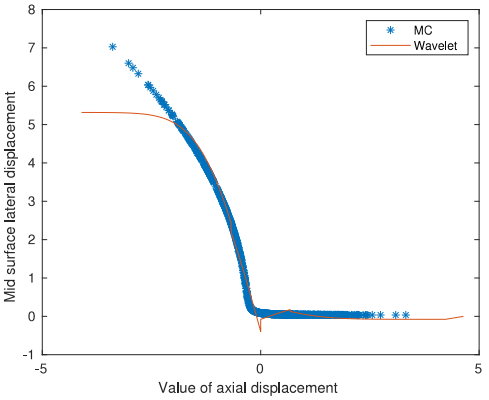

(a) Comparison of the distribution of the tip displacement using wavelet expansion and Monte Carlo.

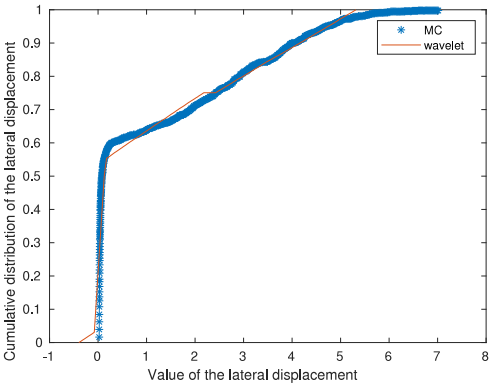

(b) Comparison of the CDF of the tip displacement using wavelet expansion and Monte Carlo.

Fig. 8. Performance of the wavelet expansion in capturing discontinuous behaviour.

for an analytical representation of the distribution). The standard deviation of the x-displacement ranges between 0.044 for the case with radial uncertainties at every cardinal point and 0.031 when the displacement at point E is deterministic. Finally, in the case where only y-displacements are imposed at points N and S, the standard deviation is several orders of magnitude smaller (6.85×10^{-4}). This standard deviation is different from zero because (i) the mesh is not symmetric, (ii) the Poisson's ratio introduces a coupling between y-displacement at the cardinal points and the x-displacement at the centre. Fig. 9(b) indicates that the removal of the stochastic y-displacement at point N decreases the standard deviation of the distribution of the y-displacement at the centre of the disc. As could be expected, suppressing the stochastic boundary condition at point E only contributes lightly to the narrowing of the output distribution as the yellow and red curves are almost superimposed.

On a final note, while this example actually deals with stochasticity of nodal displacement, a straightforward extension to nodal reference coordinate stochasticity (and thus, reference frame geometrical stochasticity) can be achieved by correcting the deformation gradient tensor, at any subsequent time, by the one after displacement stochasticity is applied (through multiplicative decomposition), thus ensuring a deformation gradient tensor equal to identity (in stochastic terms)—and thus a zero stress tensor—with nodal position defined stochastically.

5. Conclusion

In this paper, a buckling problem of a 3D beam with stochastic boundary conditions was first proposed using an intrusive method relying on an uncertainty propagation scheme. The solution was expanded as the sum of

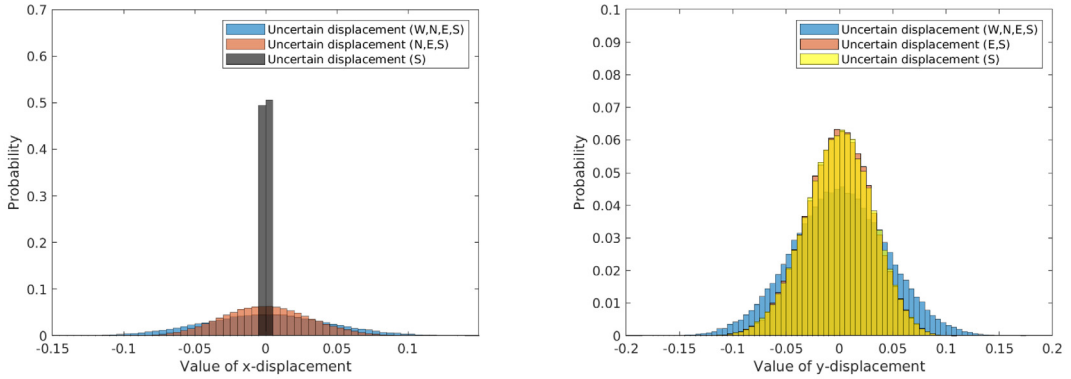

(a) Distribution of the x displacement of the center of the circle for scenarii with different magnitudes of uncertainties.

(b) Distribution of the y displacement of the center of the circle for scenarii with different magnitudes of uncertainties.

Fig. 9. Distribution of the x–y displacement of the centre of the circle for scenarios with different magnitudes of uncertainties. (For interpretation of the references to colour in this figure legend, the reader is referred to the web version of this article.)

probabilistic functions dependent on the probability distribution of the inputs. Three families of expansion were studied: the PCE, built on smooth functions, the Haar expansion involving discontinuous functions and the wavelet expansion where both smooth and discontinuous functions are used. To the best of our knowledge, this is the first time the two latter expansions have been used in a stochastic finite element method code. The main drawback of these approaches is that they all require coding efforts as the governing equations have to be modified, with a potentially significant increase of nodal degrees of freedom, making the use of commercial software, at the very least, cumbersome. Such effort is however compensated by an increased efficiency when compared to the more naive approach based on MC simulations. To facilitate this endeavour, a modular approach is proposed here where a library performing stochastic operations is plugged into a finite element code to allow, in combination with minor modifications in the core of the solver, for the simulations of stochastic problems.

In the illustrative idealised buckling problem adopted here, the predicted lateral tip displacement exhibits an abrupt change of slopes with respect to the stochastic input data when going from compressive to tensile longitudinal displacement. The PCE approach is shown to be inefficient to capture this behaviour with no obvious convergence pattern. The Haar expansion, while providing more satisfying results, suffers from a very slow convergence, thus in the need of a higher order for the expansions, and as such, of a larger number of degree of freedoms. Finally, the wavelet approach results in a very good match with a moderate increase of number of degree of freedoms with a computational time reduced by a factor three compared to the MC approach.

The second problem provides a workable computational basis for uncertainty estimation of one or multiple—a priori inaccessible—physical locations in structural components by evaluation of displacement of other—potentially more accessible—material points. The provided disc example's results are intuitively demonstrating that the more points one knows on the circumference of the disc, the more accurate the knowledge of the position of its centre O will be. In particular, standard deviations were found to drop by $\sim$25% with the knowledge of the zero-displacement of only one cardinal point. While more work to make such method scalable is needed, it holds important promises for in silico in-service structure evaluations.

Finally, it is worth emphasising that our mathematical formulation takes into account the fact that the density and material properties can be stochastic variables, though it was not tested here in this idealised problem. It is thus possible to simulate, among others, problems involving stochastic porosity (of relevance to materials manufactured using high pressure die casting for example) or any other material with non-homogenised properties.

Declaration of competing interest

The authors declare that they have no known competing financial interests or personal relationships that could have appeared to influence the work reported in this paper.

Acknowledgement

The authors acknowledge funding by the EPSRC Prosperity Partnership, UK Grant EP/S005072/1.

Appendix A

This appendix details (i) the algebra used to perform operations on stochastic quantities, (ii) the derivation of the tangent modulus for the stochastic Saint Venant–Kirchhoff model, (iii) the closed form of the PCE with Gaussian distributed uncertainties.

A.1. Stochastic algebra

While this distinction was not made in the manuscript for readability, here, the stochastic variables are defined with the $\hat{}$ symbol, while their deterministic counterparts are not.

A.1.1. Linear combination of real numbers and stochastic variable

Let us consider a stochastic variable $\hat{A}$ with coordinates $[a_1, \ldots, a_\zeta]$ in the stochastic space $\mathrm{H} = [\Psi_1, \ldots, \Psi_\zeta]$, and two real numbers f and g. $\hat{B} = f\hat{A}\hat{+}g$ can be expressed as follows:

$$\hat{B} = \sum_{\alpha=1}^{\zeta} f a_\alpha \Psi_\alpha + g. \tag{36}$$

As $\Psi_1 = 1$, the coordinates of $\hat{B}$ in the stochastic space are $[fa_1+g, fa_2, \ldots, fa_\zeta]$. The definition of $\hat{-}$ follows trivially. Note also that the extension of $\hat{+}$ and $\hat{-}$ to the linear combination of two stochastic variables is trivial.

A.1.2. Product of two stochastic variables

As the direct product of two stochastic variables belonging to H does not necessarily belong to H, we define here the stochastic product $\hat{\times}$ by projection on H. As such, for a stochastic variable $\hat{A}$ of coordinates $[a_1, \ldots, a_\zeta]$ and $\hat{B}$ of coordinates $[b_1, \ldots, b_\zeta]$, the stochastic product $\hat{D} = \hat{A}\hat{\times}\hat{B}$ with $\hat{D} = [d_1, \ldots, d_\zeta]$ in H is defined by Galerkin projection of the quantity $\left(\sum_{\alpha=1}^{\zeta} a_\alpha \Psi_\alpha\right) \times \left(\sum_{\beta=1}^{\zeta} b_\beta \Psi_\beta\right)$, i.e.,

$$d_\gamma \langle \Psi_\gamma, \Psi_\gamma \rangle = \sum_{\alpha=1}^{\zeta}\sum_{\beta=1}^{\zeta} a_\alpha b_\beta \langle \Psi_\alpha \Psi_\beta, \Psi_\gamma \rangle, \quad \forall \gamma \in [1, \zeta]. \tag{37}$$

Noting $C_{\alpha\beta\gamma} = \frac{\langle \Psi_\alpha \Psi_\beta, \Psi_\gamma \rangle}{\langle \Psi_\gamma, \Psi_\gamma \rangle}$, Eq. (37) becomes:

$$d_\gamma = \sum_{\alpha=1}^{\zeta}\sum_{\beta=1}^{\zeta} C_{\alpha\beta\gamma} a_\alpha b_\beta, \quad \forall \gamma \in [1, \zeta]. \tag{38}$$

The tensor $\boldsymbol{C}$ is a key element of the stochastic algebra and is unique to each interpolation basis. It only needs to be computed once.

A.1.3. Division of two stochastic variables

The division of $\hat{A}$ by $\hat{B}$, noted here as $\hat{D} = \hat{A}\hat{\div}\hat{B}$, can be recast as $\hat{A} = \hat{D} \;\hat{\times}\; \hat{B}$ where the coordinates of $\hat{D}$ in H have to be determined. This is thus equivalent to solving the linear system $\mathscr{C} \cdot \hat{D} = \hat{A}$, where the coefficient of $\mathscr{C}$ are defined as follows:

$$\mathscr{C}_{\beta\gamma} = \sum_{\alpha=0}^{\zeta} b_\alpha C_{\alpha\gamma\beta}. \tag{39}$$

A.1.4. Product of a stochastic variable and a stochastic tensor

Using the same approach, the coordinates $[\boldsymbol{d}_1, \ldots, \boldsymbol{d}_\zeta]$ of the product $\hat{\boldsymbol{D}} = \hat{\boldsymbol{A}} \hat{\times} \hat{B}$ between a stochastic tensor $\hat{\boldsymbol{A}}$ of coordinates $[\boldsymbol{a}_1, \ldots, \boldsymbol{a}_\zeta]$ and a stochastic variable $\hat{B}$ of coordinates $[b_1, \ldots, b_\zeta]$ are straightforwardly defined by:

$$\boldsymbol{d}_\gamma = \sum_{\alpha=0}^{\zeta} C_{\alpha\beta\gamma} \boldsymbol{A}_\alpha b_\beta, \quad \forall \gamma \in [1, \zeta]. \tag{40}$$

Note that this product is commutative as $\boldsymbol{C}$ is symmetric on its two first indices.

A.1.5. Product of two stochastic tensors

Similarly, the coordinates $[\boldsymbol{d}_1, \ldots, \boldsymbol{d}_\zeta]$ of the product $\hat{\boldsymbol{D}} = \hat{\boldsymbol{A}} \hat{\cdot} \hat{\boldsymbol{B}}$ between two stochastic tensors $\hat{\boldsymbol{A}}$ and $\hat{\boldsymbol{B}}$ of coordinates $[\boldsymbol{a}_1, \ldots, \boldsymbol{a}_\zeta]$ and $[\boldsymbol{b}_1, \ldots, \boldsymbol{b}_\zeta]$ are defined by:

$$\boldsymbol{d}_\gamma = \sum_{\alpha=0}^{\zeta} C_{\alpha\beta\gamma} \boldsymbol{a}_\alpha \cdot \boldsymbol{b}_\beta, \quad \forall \gamma \in [1, \zeta]. \tag{41}$$

Again, this product is commutative.

A.1.6. Trace of a stochastic tensor

The coordinates $[b_1, \ldots, b_\zeta]$ of the trace $\hat{B} = \hat{tr}(\hat{\boldsymbol{A}})$ of a stochastic tensor $\hat{\boldsymbol{A}}$ of coordinates $[\boldsymbol{a}_1, \ldots, \boldsymbol{a}_\zeta]$ are defined by:

$$b_\beta = tr(\boldsymbol{A}_\beta), \quad \forall \beta \in [1, \zeta]. \tag{42}$$

A.2. Tangent modulus derivation

This subsection presents the complete derivation of the partial derivative terms in Eq. (22) when using a Saint Venant–Kirchhoff constitutive model with stochastic material properties.

A.2.1. Derivation of $\frac{\partial P^\iota_{iJ}}{\partial F^\omega_{qM}}$

The term P^ι_{iJ} can be written as:

$$P^\iota_{iJ} = C_{\alpha\beta\iota} F^\alpha_{iK} S^\beta_{KJ} \tag{43}$$

Consequently, the term $\frac{\partial P^\iota_{iJ}}{\partial F^\omega_{qM}}$ can be written as follows:

$$\frac{\partial P^\iota_{iJ}}{\partial F^\omega_{qM}} = C_{\alpha\beta\iota} \left(\frac{\partial F^\alpha_{iK}}{\partial F^\omega_{qM}} S^\beta_{KJ} + F^\alpha_{iK} \frac{\partial S^\beta_{KJ}}{\partial F^\omega_{qM}} \right) \tag{44}$$

A.2.2. Derivation of $\frac{\partial S^\beta_{KJ}}{\partial F^\omega_{qM}}$

Making use of the operators defined above, Eq. (24) can be written as follows:

$$S^\beta_{KJ} = C_{\gamma\zeta\beta}(2\mu^\gamma E^\zeta_{KJ} + \lambda^\gamma E^\zeta_{XX} \delta_{KJ}) \tag{45}$$

The term $\frac{\partial S^\beta_{KJ}}{\partial F^\omega_{qM}}$ can be written as:

$$\frac{\partial S^\beta_{KJ}}{\partial F^\omega_{qM}} = \frac{\partial S^\beta_{KJ}}{\partial E^\psi_{RS}} \frac{\partial E^\psi_{RS}}{\partial F^\omega_{qM}} \tag{46}$$

Using the symmetry of the spatial indices of the tensor $\boldsymbol{E}$, the term $\frac{\partial S^\beta_{KJ}}{\partial E^\psi_{RS}}$ can be written as:

$$\frac{\partial S^\beta_{KJ}}{\partial E^\psi_{RS}} = C_{\gamma\zeta\beta}(\mu^\gamma \delta_{\zeta\psi}(\delta_{KR}\delta_{JS} + \delta_{SK}\delta_{JR}) + \lambda^\gamma \delta_{\zeta\psi}\delta_{RS}\delta_{KJ}) \tag{47}$$

This equation can further be simplified as:

$$\frac{\partial S^{\beta}_{KJ}}{\partial E^{\psi}_{RS}} = C_{\gamma\psi\beta}(\mu^{\gamma}(\delta_{KR}\delta_{JS} + \delta_{SK}\delta_{JR}) + \lambda^{\gamma}\delta_{RS}\delta_{KJ}) \tag{48}$$

The last term to determine is $\frac{\partial E^{\psi}_{RS}}{\partial F^{\omega}_{qM}}$. The expression of E^{ψ}_{RS} is:

$$E^{\psi}_{RS} = \frac{1}{2}C_{\chi\varphi\psi}(F^{\chi}_{nR}F^{\varphi}_{nS} - \delta_{RS}\delta_{1\psi}) \tag{49}$$

Consequently, the term $\frac{\partial E^{\psi}_{RS}}{\partial F^{\omega}_{qM}}$ can be written as:

$$\frac{\partial E^{\psi}_{RS}}{\partial F^{\omega}_{qM}} = \frac{1}{2}C_{\chi\varphi\psi}(\delta_{nq}\delta_{\chi\omega}\delta_{RM}F^{\varphi}_{nS} + \delta_{nq}\delta_{\varphi\omega}\delta_{SM}F^{\chi}_{nR}) \tag{50}$$

and eventually as:

$$\frac{\partial E^{\psi}_{RS}}{\partial F^{\omega}_{qM}} = \frac{1}{2}(C_{\omega\varphi\psi}\delta_{RM}F^{\varphi}_{qS} + C_{\chi\omega\psi}\delta_{SM}F^{\chi}_{qR}) \tag{51}$$

As a result, the term $\frac{\partial S^{\beta}_{KJ}}{\partial F^{\omega}_{qM}}$ can finally be expressed as:

$$\frac{\partial S^{\beta}_{KJ}}{\partial F^{\omega}_{qM}} = \frac{1}{2}C_{\gamma\psi\beta}\left(\mu^{\gamma}\left(\delta_{KR}\delta_{JS} + \delta_{SK}\delta_{JR}\right) + \lambda^{\gamma}\delta_{RS}\delta_{KJ}\right)\left(C_{\omega\varphi\psi}\delta_{RM}F^{\varphi}_{qS} + C_{\chi\omega\psi}\delta_{SM}F^{\chi}_{qR}\right) \tag{52}$$

A.2.3. Derivation of $\frac{\partial P^{\iota}_{iJ}}{\partial F^{\omega}_{qM}}\frac{\partial F^{\omega}_{qM}}{\partial u^{\epsilon}_{kb}}$

Using Eq. (23), the term $\frac{\partial P^{\iota}_{iJ}}{\partial F^{\omega}_{qM}}\frac{\partial F^{\omega}_{qM}}{\partial u^{\epsilon}_{kb}}$ can be written as:

$$\frac{\partial P^{\iota}_{iJ}}{\partial F^{\omega}_{qM}}\frac{\partial F^{\omega}_{qM}}{\partial u^{\epsilon}_{kb}} = \frac{\partial P^{\iota}_{iJ}}{\partial F^{\omega}_{qM}}\delta_{qk}N_{b,M}\delta_{\epsilon\omega} = \frac{\partial P^{\iota}_{iJ}}{\partial F^{\epsilon}_{kM}}N_{b,M} \tag{53}$$

which, noting that

$$\frac{\partial F^{\alpha}_{iK}}{\partial F^{\epsilon}_{kM}} = \delta_{ik}\delta_{\alpha\epsilon}\delta_{KM}, \tag{54}$$

can then be further expanded as:

$$\begin{aligned}
&\frac{\partial P^{\iota}_{iJ}}{\partial F^{\epsilon}_{kM}}N_{b,M} = C_{\alpha\beta\iota}\left(\frac{\partial F^{\alpha}_{iK}}{\partial F^{\epsilon}_{kM}}S^{\beta}_{KJ} + F^{\alpha}_{iK}\frac{\partial S^{\beta}_{KJ}}{\partial F^{\epsilon}_{kM}}\right)N_{b,M} = \\
&C_{\alpha\beta\iota}\left(\delta_{ik}\delta_{\alpha\epsilon}S^{\beta}_{MJ} + F^{\alpha}_{iK}\frac{1}{2}C_{\gamma\psi\beta}\left(\mu^{\gamma}\left(\delta_{KR}\delta_{JS} + \delta_{SK}\delta_{JR}\right) + \lambda^{\gamma}\delta_{RS}\delta_{KJ}\right)\left(C_{\epsilon\varphi\psi}\delta_{RM}F^{\varphi}_{kS} + C_{\chi\epsilon\psi}\delta_{SM}F^{\chi}_{kR}\right)\right)N_{b,M} = \\
&C_{\alpha\beta\iota}(\delta_{ik}\delta_{\alpha\epsilon}S^{\beta}_{MJ} + F^{\alpha}_{iK}\frac{1}{2}C_{\gamma\psi\beta}\mu^{\gamma}\delta_{KR}\delta_{JS}C_{\epsilon\varphi\psi}\delta_{RM}F^{\varphi}_{kS} + \\
&F^{\alpha}_{iK}\frac{1}{2}C_{\gamma\psi\beta}\mu^{\gamma}\delta_{KR}\delta_{JS}C_{\chi\epsilon\psi}\delta_{SM}F^{\chi}_{kR} + \\
&F^{\alpha}_{iK}\frac{1}{2}C_{\gamma\psi\beta}\mu^{\gamma}\delta_{SK}\delta_{JR}C_{\epsilon\varphi\psi}\delta_{RM}F^{\varphi}_{kS} + \\
&F^{\alpha}_{iK}\frac{1}{2}C_{\gamma\psi\beta}\mu^{\gamma}\delta_{SK}\delta_{JR}C_{\chi\epsilon\psi}\delta_{SM}F^{\chi}_{kR} + F^{\alpha}_{iK}\frac{1}{2}C_{\gamma\psi\beta}\lambda^{\gamma}\delta_{RS}\delta_{KJ}C_{\epsilon\varphi\psi}\delta_{RM}F^{\varphi}_{kS} + \\
&F^{\alpha}_{iK}\frac{1}{2}C_{\gamma\psi\beta}\lambda^{\gamma}\delta_{RS}\delta_{KJ}C_{\chi\epsilon\psi}\delta_{SM}F^{\chi}_{kR})
\end{aligned} \tag{55}$$

Simplifying the Kronecker indices, Eq. (55) becomes:

$$\begin{aligned}\frac{\partial P^{\iota}_{iJ}}{\partial F^{\epsilon}_{kM}} N_{b,M} = C_{\alpha\beta\iota}(\delta_{ik}\delta_{\alpha\epsilon} S^{\beta}_{MJ} + F^{\alpha}_{iM}\frac{1}{2}C_{\gamma\psi\beta}\mu^{\gamma}C_{\epsilon\varphi\psi}F^{\varphi}_{kJ} + F^{\alpha}_{iK}\frac{1}{2}C_{\gamma\psi\beta}\mu^{\gamma}\delta_{JM}C_{\chi\epsilon\psi}F^{\chi}_{kK} + \\ F^{\alpha}_{iK}\frac{1}{2}C_{\gamma\psi\beta}\mu^{\gamma}\delta_{JM}C_{\epsilon\varphi\psi}F^{\varphi}_{kK} + \\ F^{\alpha}_{iM}\frac{1}{2}C_{\gamma\psi\beta}\mu^{\gamma}C_{\chi\epsilon\psi}F^{\chi}_{kJ} + F^{\alpha}_{iJ}\frac{1}{2}C_{\gamma\psi\beta}\lambda^{\gamma}C_{\epsilon\varphi\psi}F^{\varphi}_{kM} + \\ F^{\alpha}_{iJ}\frac{1}{2}C_{\gamma\psi\beta}\lambda^{\gamma}C_{\chi\epsilon\psi}F^{\chi}_{kM})N_{b,M}.\end{aligned} \tag{56}$$

Using the symmetry of the third-order tensor $\boldsymbol{C}$ finally leads to:

$$\begin{aligned}\frac{\partial P^{\iota}_{iJ}}{\partial F^{\epsilon}_{kM}} N_{b,M} = C_{\alpha\beta\iota}(\delta_{ik}\delta_{\alpha\epsilon} S^{\beta}_{MJ} + F^{\alpha}_{iM}C_{\gamma\psi\beta}\mu^{\gamma}C_{\epsilon\varphi\psi}F^{\varphi}_{kJ} + F^{\alpha}_{iK}C_{\gamma\psi\beta}\mu^{\gamma}\delta_{JM}C_{\epsilon\varphi\psi}F^{\varphi}_{kK} \\ + F^{\alpha}_{iJ}C_{\gamma\psi\beta}\lambda^{\gamma}C_{\epsilon\varphi\psi}F^{\varphi}_{kM})N_{b,M}.\end{aligned} \tag{57}$$

A.3. Expansions considering Gaussian stochastic variables

In this subsection, we detail the mathematical expression of the polynomial chaos, Haar and wavelet expansions when the input parameter ϵ follows a Gaussian distribution. Following the Wiener–Askey scheme summarised in Table 1, the univariate polynomials ψ_{η} have the following expression [38]:

$$\psi_{\eta}(\epsilon) = \sum_{k=0}^{\lfloor\frac{\eta-1}{2}\rfloor}(-1)^{k}\frac{(\eta-1)!}{2^{k}k!(\eta-1-2k)!}\epsilon^{\eta-1-2k}, \tag{58}$$

where $\lfloor\rfloor$ is the floor operator.

Building the Haar and wavelet expansions requires to know the function F that links the cumulative distribution y (comprised between 0 and 1) of the variable ϵ to the value of the variable ϵ. Taking into account the fact that ϵ is a Gaussian variable, the function F can be expressed as follows:

$$F(y) = \frac{1}{2}\left(1 + erf(\frac{y}{\sqrt{2}})\right)^{-1}, \tag{59}$$

where erf is the error function. The function F in Eq. (59) can be approximated by the following formula [39]:

$$F(y) = t - \frac{2.30753 + 0.27061t}{1 + 0.99229t + 0.04481t^{2}}, \tag{60}$$

where $t = \sqrt{\ln\left(\frac{1}{(1-y)^{2}}\right)}$. This approximation is only valid when $0.5 \leq y \leq 1$ but can be extended to the interval [0,1] using the fact that $F(y) = -F(1-y)$.

Appendix B. Supplementary data

Supplementary material related to this article can be found online at https://doi.org/10.1016/j.cma.2022.115044. C++ libraries of the stochastic algebra are provided with the online publication. The open access in-house code MuPhiSim was used for the simulations.

References

[1] K. Dou, E. Lordan, Y. Zhang, A. Jacot, Z. Fan, A novel approach to optimize mechanical properties for aluminium alloy in high pressure die casting (HPDC) process combining experiment and modelling, J. Mater Process. Technol. 296 (2021).
[2] X. Li, L. Zhang, Y. Dong, Z. Wei, Z. Que, X. Qu, Orientation relationship of texture development in hot-rolled W during annealing, Int. J. Refract. Met. Hard Mater. 97 (2021) 105527.
[3] T. Mesogitis, A. Skordos, A. Long, Uncertainty in the manufacturing of fibrous thermosetting composites: A review, Composites A 57 (2014) 67–75.
[4] P. Love, R. Lopez, Y. Goh, C. Tam, What goes up, shouldn't come down: Learning from construction and engineering failures, Procedia Eng. 14 (2011) 844–850.

[5] J. Bigen, Durability of Engineering Structures: Design, Repair and Maintenance, Woodhead Publishing, 2003.
[6] B. Rao, Revisiting classical design in engineering from a perspective of frugality, Heliyon 3 (5) (2017) e00299.
[7] J.-S. Kim, C.-G. Kim, C.-S. Hong, T. Hahn, Development of concurrent engineering system for design of composite structures, Compos. Struct. 50 (3) (2000) 297–309.
[8] R. Caflisch, Monte Carlo and quasi-Monte Carlo methods, Acta Numer. 7 (1998) 1–49.
[9] N. Weiner, The homogeneous chaos, Amer. J. Math. 60 (4) (1938) 897–936.
[10] R. Ghanem, P. Spanos, Stochastic Finite Elements: A Spectral Approach, Springer-Verlag, 1991, 0.
[11] D. Xiu, G. Karniadakis, The Wiener-Askey polynomial chaos for stochastic differential equations, SIAM J. Sci. Comput. 24 (2002) 619–644.
[12] B. Rosic, M. Hermann, Variational theory and computations in stochastic plasticity, Arch. Comput. Methods Eng. 22 (2015) 457–509.
[13] S. Huang, M. Sankaran, R. Ramesh, Collocation-based stochastic finite element analysis for random field problems, Probab. Eng. Mech. 22 (2007) 194–205.
[14] G. Blatman, B. Sudret, Adaptive sparse polynomial chaos expansion based on least angle regression, J. Comput. Phys. 230 (6) (2011) 2345–2367.
[15] G. Stefanou, The stochastic finite element method: Past present and futures, Comput. Methods Appl. Mech. Engrg. 1998 (2009) 1031–1051.
[16] M. Eiermann, O. Ernst, E. Ullmann, Computational aspects of the stochastic finite element method, Comput. Vis. Sci. 10 (2007) 3–15.
[17] S. Acharjee, N. Zabaras, Uncertainty propagation in finite deformations—-A spectral stochastic Lagrangian approach, Comput. Methods Appl. Mech. Engrg. 195 (2006) 2289–2312.
[18] A. Nouy, F. Schoefs, N. Moës, X-SFEM, a computational technique based on X-FEM to deal with random shapes, Eur. J. Comput. Mech. 16 (2) (2007) 277–293.
[19] C. Daux, N. Moës, J. Dolbow, N. Sukumar, T. Belytschko, Arbitrary branched and intersecting cracks with the extended finite element method, Internat. J. Numer. Methods Engrg. 48 (12) (2000) 1741–1760.
[20] S. Sakata, F. Ashida, K. Enya, A microscopic failure probability analysis of a unidirectional fiber reinforced composite material via a multiscale stochastic stress analysis for a microscopic random variation of an elastic property, Comput. Mater. Sci. 62 (2012) 35–46.
[21] F.-Y. Zhu, S. Jeong, H. Lin, G. Yun, Probabilistic multiscale modeling of 3D randomly oriented and aligned wavy CNT nanocomposites and RVE size determination, Compos. Struct. 195 (2018) 265–275.
[22] D. Pivovarov, P. Steinman, Modified SFEM for computational homogenization of heterogeneous materials with microstructural geometric uncertainties, Comput. Mech. 57 (2016).
[23] V. Nair, S. Sarkar, R. Sujith, Uncertainty quantification of subcritical bifurcations, Probab. Eng. Mech. 34 (2013) 177–188.
[24] O. Le Maitre, H. Najm, R. Ghanem, Multi-resolution analysis of Wiener-type uncertainty propagation schemes, J. Comput. Phys. 197 (2004) 502–531.
[25] G. Helmberg, The Gibbs phenomenon for Fourier interpolation, J. Approx. Theory 78 (1) (1994) 41–63.
[26] O. Le Maitre, O. Knio, H. Najm, R. Ghanem, Uncertainty propagation using Wiener–Haar expansions, J. Comput. Phys. 197 (2004) 28–57.
[27] M. Rocas, A. García-González, X. Larráyoz, Nonintrusive stochastic finite elements for crashworthiness with VPS/Pamcrash, Arch. Comput. Methods Eng. 27 (2020) 1337–1362.
[28] R. Cameron, W. Martin, Transformations of Wiener integrals under translations, Ann. of Math. 45 (1944) 386–396.
[29] D. Walnut, An introduction to wavelets analysis, Appl. Numer. Harmon. Anal. (2002).
[30] B. Alpert, A class of bases in L 2 for the sparse representation of integral operators, SIAM J. Math. Anal. (1993) 246–262.
[31] Q. Zhiping, Z. Zhang, Fatigue crack propagation analysis in structures with random parameters based on polynomial chaos expansion method, Theor. Appl. Fract. Mech. 105 (2020).
[32] L. Cam, The central limit theorem around 1935, Statist. Sci. 1 (1) (1986) 78–91.
[33] H. Rappel, L. Beex, L. Noels, Identifying elastoplastic parameters with Bayes' theorem considering output error, input error and model uncertainty, Probab. Eng. Mech. 55 (2019) 28–41.
[34] Y. Chien, K. Fu, On the generalized Karhunen–Loève expansion, IEEE Trans. Inform. Theory 13 (1967) 518–520.
[35] A. Bakushinskii, A numerical method for solving fredholm integral equations of the 1st kind, USSR Comput. Math. Math. Phys. 5 (4) (1965) 226–233.
[36] K. Phoon, H. Huang, S. Quek, Simulation of strongly non-Gaussian processes using karhunen–loeve expansion, Probab. Eng. Mech. 20 (2005) 188–198.
[37] B. Debusschere, H. Najm, P. Pebay, Numerical Challenges in the Use of Polynomial Chaos Representations for Stochastic Processes, Vol. 26, Society for Industrial and Applied Mathematics, 2004, pp. 698–719.
[38] B. Saha, On a generating function of Hermite polynomial, Yokohama Math. J. (1969) 73–76.
[39] M. Abramowitz, I. Stegun, Handbook of mathematical functions with formulas, graphs, and mathematical tables, Probab. Eng. Mech. 20 (1964) 188–198.